Model for the dynamics of carrier injection in a band with polaronic states: Application to exciton dissociation in organic solar cells

Khouloud Chika, Alexandre Perrin, Jouda Jemaa Khabthani, Ghassen Jemaï, Jean-Pierre Julien, Samia Charfi Kaddour, Didier Mayou

Model for the dynamics of carrier injection in a band with polaronic states: Application to exciton dissociation in organic solar cells

Khouloud Chika,[1,*] Alexandre Perrin,[2] Jouda Jemaa Khabthani,[1] Ghassen Jemaï,[1] Jean-Pierre Julien,[2] Samia Charfi Kaddour,[1] and Didier Mayou[2]

[1]*Université Tunis El Manar, Faculté des Sciences de Tunis, Laboratoire de Physique de la Matiére Condensée, 1060 Tunis, Tunisia*
[2]*Université Grenoble Alpes, CNRS, Institut NÉEL, F-38042 Grenoble, France*

(Received 20 April 2022; revised 6 October 2022; accepted 25 October 2022; published 22 November 2022)

We develop a quantum model for the dynamics of carrier injection in a band that presents a strong carrier-vibration coupling. This coupling modifies the spectral density of the band and can even create pseudogaps that signal the onset of polaronic states. The injection of a carrier that interacts with many vibration modes is a complex many-body process that is treated by combining the quantum scattering theory and the dynamical mean-field theory (DMFT). For the model analyzed here, which is adapted to compact phases, the number Z of neighbors of a given site is large and in this limit the DMFT becomes exact. The model is applied to the excitonic dissociation at the donor-acceptor interface for organic solar cells. The main ingredients are the electron-hole Coulomb interaction, the recombination process, and the existence of polaronic states in the acceptor band. Using parameters extracted from *ab initio* calculations we analyze the spectral density on the charge transfer state (CTS), the average energy transferred to phonons on the CTS, and the quantum yield of the injection process. We find in particular that even with a strong electron-vibration coupling, one can get a vibrationally cold charge transfer state with a high injection yield as often observed experimentally.

DOI: 10.1103/PhysRevB.106.195420

The interfacial charge transfer between heterogeneous materials constitutes a key physical phenomenon central to a variety of light-induced energy transport and conversion processes such as photocatalysis, photovoltaics, energy storage, and molecular electronics [1–8]. In the case of excitonic solar cells such as heterojunction bulk organic solar cells the photon is absorbed in the donor zone and leads to the creation of an exciton which is stable because of the strong Coulomb interaction between the electron and the hole constituting it. The exciton must migrate to the donor-acceptor interface in order to dissociate [9,10]. Yet once the charges are in separate phases, they still need to overcome their mutual Coulomb attraction which is larger than the thermal energy room (around 0.025 eV); otherwise they recombine [11–15]. Several phenomena have been identified as facilitators of charge separation such as built-in electric fields at donor-acceptor interfaces, delocalization of the excitons and of the free carrier charges, the offset in energy levels between donor and acceptor, and structural disorder [16–22]. A central concept is that of the charge transfer state (CTS) which is the first state in which the electron hops on the acceptor side and on which it is coupled to local vibration modes. Because of this coupling, the electron can excite one or several phonons of the vibration mode which corresponds to a vibrationally hot CTS. If no phonons are excited this corresponds to a vibrationally cold CTS. A much-debated issue is how the efficiency of the charge separation is related to the release of energy on these modes (vibrationally hot CTS) or not (vibrationally cold CTS) [19,23–30].

On the theoretical side, the treatment of charge transfer in organic semiconductors is complex. Historically some phenomenological models were developed such as the Braun-Onsager [31,32] analytic model which is based on a classical picture that allows one to describe separation in a strong Coulomb potential. The Marcus theory and related approaches are also much used and describe charge transfer at the molecular level with incoherent hopping [19,20,33–37]. *Ab initio* electronic structure calculations [21,22,38] also bring much useful information concerning the electronic states and the electrostatic potential. For a fully microscopic understanding of the charge separation mechanism in these organic photovoltaic devices, numerical methods have been proposed such as exact diagonalization [39] and time-dependent density functional theory [40–42]. Yet the problem of describing properly the charge separation process is still largely open and new complementary approaches are needed.

In the present study, we develop a formalism for the analysis of carrier injection in a band with polaronic states. The injection of a carrier that interacts with many vibration modes is a complex many-body process that is treated by combining the quantum scattering theory and the dynamical mean-field theory (DMFT). This avoids perturbative theories, such as the Fermi golden rule [43,44], which is often used but is justified only at the weak electron-vibration coupling. This mean-field approach becomes exact for models with a number Z of neighbors which becomes large and is therefore well adapted to compact systems. We apply it to the dynamics of the exciton dissociation process in organic solar cells. For

*khouloud.chika@fst.utm.tn

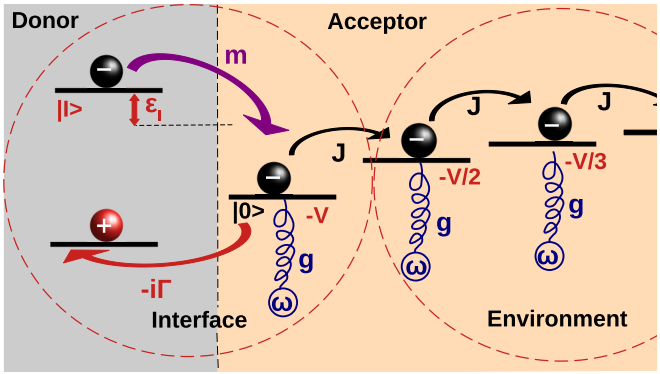

FIG. 1. Representation of the model. $|I\rangle$ is the initial state when the electron is on the LUMO orbital on the donor side. $|0\rangle$ is the state when the electron is on the CTS ($L = 0$) where it can recombine with a rate Γ. The electron propagates through the different layers $L = 0, 1, 2, \ldots$ and can excite the local vibration modes.

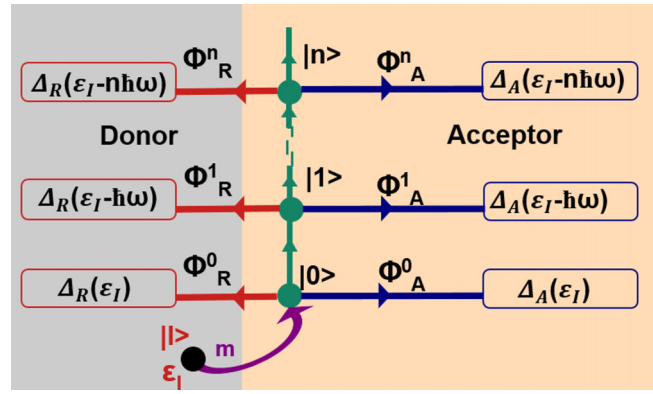

FIG. 2. Schematic representation for the charge injection process in the Hilbert space. Φ_R^n are the recombination fluxes that enter the recombination channels and Φ_A^n are the injection fluxes that enter in the injection channels (acceptor side). The values of the fluxes are determined from the self-energies $\Delta_R(\varepsilon_I - n\hbar\omega)$ and $\Delta_A(\varepsilon_I - n\hbar\omega)$ as explained in the SM.

simplicity, we consider only one band on the acceptor side and retain only the excitonic state on the donor side which couples most efficiently to charge transporting states [19]. We use a simple Holstein Hamiltonian which describes an electron that interacts with one mode on each site of the acceptor. All the modes are equivalent and have the same frequency and the same coupling to the electron. In addition, we include the electrostatic potential due to the electron-hole interaction near the donor-acceptor interface. On the acceptor side, we do not include a disorder potential whose effect on the injection process can be moderate as shown in [45]. A typical range for the parameters of the Hamiltonian is estimated from *ab initio* calculations [26–29,46]. We analyze the spectral density on the CTS, the energy released by emission of phonons on the CTS, and the quantum yield. We establish in particular a phase diagram for the energy released on the CTS and the quantum yield as a function of the injection energy and of the recombination rate. We find that in the presence of the electron-hole attraction, the electron can be injected into the acceptor with moderate initial energy and we show that the charge transfer state can stay vibrationally cold [19,23] with a high yield even with a strong electron-vibration coupling.

Our charge separation model is presented in Fig. 1. We consider optical modes with frequencies higher than the thermal energy at room temperature so that all vibration modes are initially empty when the charge injection process starts. The red ball is the hole that is considered fixed and the black balls represent the different positions of the electron. The state $|I\rangle$ is the excited singlet state from which the electron can be injected into the charge transfer state (CTS) via the hopping integral m. In this state $|I\rangle$, the electron is on the LUMO orbital on the donor side and the hole is on the HOMO orbital. The electron can jump, on the sites i of the successive layers $L = 0, 1, 2, \ldots$ (the layer $L = 0$ is the CTS itself), and it can excite phonons on all sites of a given layer. We assume that the sites i are distributed on a Bethe lattice [47,48] which is known to reproduce correctly the local environment of a compact system (see the Supplemental Material (SM) [49]). For simplicity, we take the standard limit of infinite coordination of this Bethe lattice, in which case the mean-field solution given by the DMFT is exact.

In this paper the total Hamiltonian H takes the form [50,51]

$$H = \varepsilon_I c_I^+ c_I - m(c_I^+ c_0 + c_0^+ c_I) - \sum_i \frac{V}{L_i + 1} c_i^+ c_i + \sum_i \hbar\omega a_i^+ a_i - \sum_{i,j} J_{i,j}(c_i^+ c_j + c_j^+ c_i) + \sum_i g_i c_i^+ c_i (a_i^+ + a_i) + H_R, \quad (1)$$

where the index i denotes the different sites, $i = 0$ being the CTS. ε_I is the energy of the incoming electron of a molecule at the donor site. The hopping parameter m between the donor site and the CTS will be taken as weak compared to the pure electronic bandwidth $4J$ so that we can take the limit $m \to 0$. For a site i the electron creation (annihilation) operators are c_i^+ (c_i). The electrostatic potential at site i which is on the layer L_i is $-\frac{V}{L_i+1}$. It is due to the electron-hole interaction and is characterized by the parameter V. The phonon creation (annihilation) operator of the local vibration mode at site i is a_i^+ (a_i) and $\hbar\omega$ is the phonon energy. $J_{i,j}$ are the hopping matrix elements between nearest neighbors i and j on the Bethe lattice and are expressed from J as explained in the SM. g is the electron-vibration coupling parameter. The Hamiltonian H_R represents the recombination processes.

The injection process is analyzed in the full Hilbert space of the electron + vibration modes system (represented in Fig. 2). The initial state $|I\rangle$ corresponds to the electron on the donor side with no vibration mode excited. The hopping term m allows the transfer to the CTS with zero phonons $|0\rangle$. Then the electron-vibration coupling couples the states $|0\rangle, |1\rangle, \ldots, |n\rangle$ with n phonons created on the CTS and no other mode excited on the acceptor side. Starting from state $|n\rangle$ there are two channels in which the electron leaves the CTS. Channel nA corresponds to the propagation on the acceptor side and channel nR corresponds to the recombination process. The probabilities of injection in channels nA (nR) are

Φ_A^n (Φ_R^n). From these quantities, it is possible to express the quantum yield Y which is the probability for the electron to be injected into the acceptor and the average vibration energy E_{TS} on the CTS [52]. One has

$$Y = \sum_{n=0}^{\infty} \Phi_A^n = 1 - \sum_{n=0}^{\infty} \Phi_R^n, \tag{2a}$$

$$E_{TS} = \sum_n n\hbar\omega\left[\Phi_A^n + \Phi_R^n\right]. \tag{2b}$$

The probabilities Φ_A^n and Φ_R^n of injection in the channels nA and nR are computed from the scattering theory [39,53–56] and depend only on the self-energies $\Delta_A(\varepsilon_I - n\hbar\omega)$ and $\Delta_R(\varepsilon_I - n\hbar\omega)$ which represent the effect of the corresponding channels. As shown in the SM, $\Delta_A(z)$ is computed from the DMFT.

Solving the coupled mean-field equations for an inhomogeneous model, as for the case with electron-hole interaction, is difficult with standard methods. In order to solve these equations, we use development in continued fractions which is very efficient [56]. In this approach, the self-energy $\Delta_A(z)$ is represented by a continued fraction with a finite number of stages N (N is up to 2000) and the energy resolution improves when N increases. Mathematically the real and imaginary parts of $\Delta_A(z)$ are related so that one has only to reconstruct the imaginary part. For a finite continued fraction with N stages the imaginary part is a sum of N delta peaks with $\mathrm{Im}\Delta_A(z) = \sum p_i\delta(E - E_i)$. In order to limit numerical fluctuations, we convolute each delta peak by a Gaussian function with an adjustable width ΔE which determines the energy resolution (see SM for more details). Physically such a broadening can be seen as reproducing a small coupling to other degrees of freedom not considered in the Hamiltonian. Here the resolution is estimated in the range $0.1J$–$0.2J$ which is sufficient for the present discussion.

The recombination process is modeled as an injection into a continuum and we discuss two limits where this continuum is either narrow with a width comparable to the electronic acceptor band (of the order of $4J$) or is much wider. We expect that the wideband limit is valid if the hole and the electron recombine by emission of a photon whose energy is larger than $4J$. This wideband limit can be a good approximation for other recombination pathways since the total energy of a few eV that is released is again larger than the typical bandwidth of the acceptor $4J$. For a recombination process into a wide continuum, we neglect the dependence of $\Delta_R(z)$ with z and for simplicity, we take $\Delta_R(z) = -i\hbar\Gamma$ where Γ is the recombination rate.

We discuss now the results obtained for the local density of states (LDOS) on the site $|0\rangle$, the energy E_{TS} lost by the electron on the CTS, and the quantum yield Y of the injection. All energies are given in units of J (the pure electronic bandwidth is $4J$) and for all cases, we consider $\hbar\omega = 1$. The LDOSs are given in units of $1/J$. We consider four cases that combine $g = 1$ or $g = \sqrt{2}$ for the electron-vibration coupling parameter with $V = 0$ or $V = 1.5$ for the electrostatic potential parameter [see the expression of the Hamiltonian in Eq. (1)]. Additional results for other values of the parameters confirm the behavior discussed here (see SM).

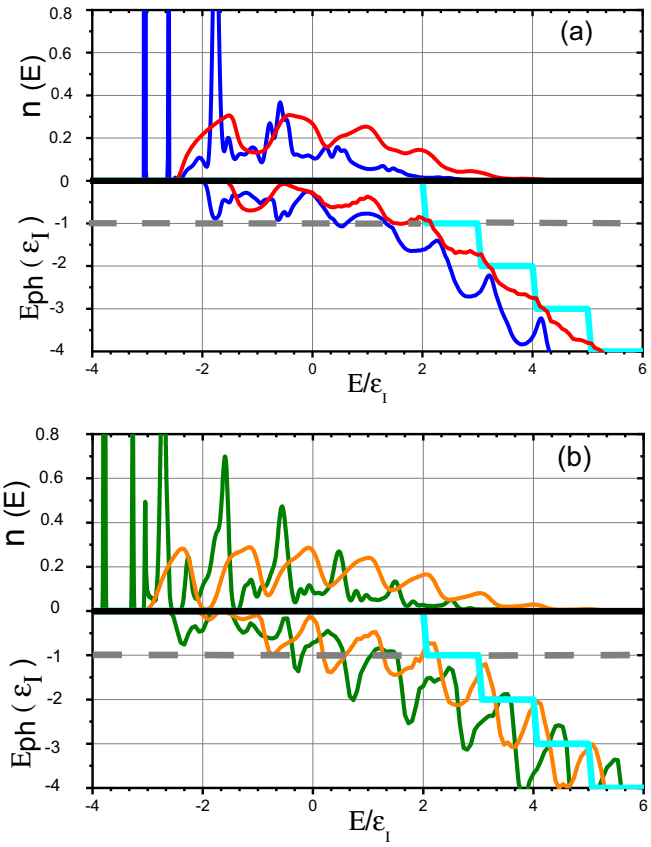

FIG. 3. The spectral density $n(E)$ and the average energy lost on the CTS $E_{ph}(\varepsilon_I)$ ($E_{ph} = -E_{TS}$) without recombination. The cyan curve represents $E_{ph}(\varepsilon_I)$ in the case where $g \to 0$. For panel (a) $g = 1$ and the potential parameter is $V = 0$ (red) and $V = 1.5$ (blue). For panel (b) $g = \sqrt{2}$ and the potential parameter is $V = 0$ (orange) and $V = 1.5$ (green). For both panels, the horizontal dashed gray line indicates the limit of vibrationally cold and hot CTS regimes.

Figure 3 presents results in the absence of recombination. We consider first the upper part of the panels (a) and (b) which show the LDOS $n(E)$ on-site $|0\rangle$. Panel (a) shows the results for $g = 1$ and for $V = 0$ (red) or $V = 1.5$ (blue). We define E_{Min} as the minimum energy of the spectrum in the bulk that is for $V = 0$. $n(E)$ tends to zero at large energies but its spectrum is infinite. $n(E)$ presents oscillations with minima separated by about $\hbar\omega = 1$ which indicates the preformation of polaronic bands. For $V = 1.5$ the electrostatic potential depends on the distance to the CTS and tends to zero far from the CTS. Therefore close to the CTS the electronic density is modified but far from the CTS one expects that the system is similar to the bulk, that is, to the case $V = 0$. For $V = 1.5$ there is a continuum part of $n(E)$ which starts at the same minimum value E_{Min} as for $V = 0$. This is expected because the states of the bulk can propagate up to the site $|0\rangle$ and give therefore contributions to the LDOS $n(E)$ for all energies $E > E_{\mathrm{Min}}$. Yet the LDOS $n(E)$ on state $|0\rangle$ is strongly modified by the electrostatic potential induced by the electron-hole interaction. In addition, there are localized states below the minimum energy E_{Min} of the bulk spectrum. These states are analogous to bound electronic states in atoms or to impurity states in semiconductors and are spatially localized

around the CTS. One may expect that there is an infinite series of such states close to $E_{\rm Min}$ but their weight is too small to be detected numerically. Yet the results indicate that the total weight of the localized states [essentially the two peaks shown in panel (a)] is about 0.34 which means that the continuum has a weight of about 0.66. This confirms that the electron-hole potential strongly modifies the LDOS. For the strongest electron-vibration coupling [$g_1 = \sqrt{2}$, in panel (b)], the two lower subbands of the continuum are nearly separated by gaps for $V = 0$ and the global width is larger than for $g = 1$. As for panel (a) the introduction of the electron-hole interaction strongly modifies the LDOS both in the continuum part and by the creation of localized states. The total weight of the localized states is about 0.20 and therefore the continuum weight is about 0.80. Note that very close to the bottom of the continuum there is a narrow peak with a small weight of about 0.01. We cannot discriminate whether this peak is below the continuum and localized or whether it belongs to the continuum, but this has no impact on our discussion.

The lower part of the panels of Fig. 3 represents the average energy $E_{ph} = -E_{TS}$ lost by emitting phonons on the CTS. In order to inject an electron into the bulk, the initial energy ε_I must be larger than the minimum energy $E_{\rm Min}$ of the bulk spectrum. Depending on ε_I two regimes occur. In the first regime there is less than one phonon emitted on average, which is a vibrationally cold transfer state regime [57] if $E_{\rm Min} < \varepsilon_I < E_{Max}$ with $E_{Max} \simeq 1.5$ for $g = 1$ and $E_{Max} \simeq 1$ for $g = \sqrt{2}$. So the range of values ε_I for injecting electrons with a vibrationally cold CTS is of about 4, i.e., close to the pure electronic bandwidth. The second regime occurs at higher values of ε_I when the electron can excite one or several phonons which correspond to a vibrationally hot CTS. The existence of these two regimes can be understood by considering the limit of small g and the energy conservation during the injection process (see Fig. 3). Indeed when ε_I is between $E_{\rm Min} = -2$ and $E_{Max} = 2$ (the values of the bounds of the continuum for the pure electronic spectrum) the system does not need to emit phonons to inject an electron in the acceptor side. But when $\varepsilon_I > E_{Max}$ it is necessary to emit a phonon prior to injecting an electron in the band and when $\varepsilon_I > 3J$ it is necessary to emit two phonons to inject electrons, and so on. This leads to the staircase curve in the lower part of panel (a). So the average energy of phonons for ε_I in the range $[E_{Max}, \infty]$ will be $E_{TS} \simeq (\varepsilon_I - E_{Max} + \hbar\omega)$. We see that the case $g = 1$ is close to $g \to 0$. For $g = \sqrt{2}$, oscillations that reflect the preformation of polaronic bands appear but the global trend is identical.

We focus now on the effect of recombination. If the recombination is treated as an injection in a narrow continuum the two channels nA and nR (see Fig. 2) correspond to narrow bands and this is a situation similar to that of Fig. 3. As discussed previously the energy conservation imposes the existence of a vibrationally hot CTS for sufficiently large ε_I. For every n the flux shares between Φ_A^n and Φ_R^n so that the yield Y is partial.

The wideband limit of the recombination is completely different as we show now. We present only the case $g = 1$ in Fig. 4 since results for $g = \sqrt{2}$ are qualitatively similar [58]. Panel (a) shows that the results are rather similar for both

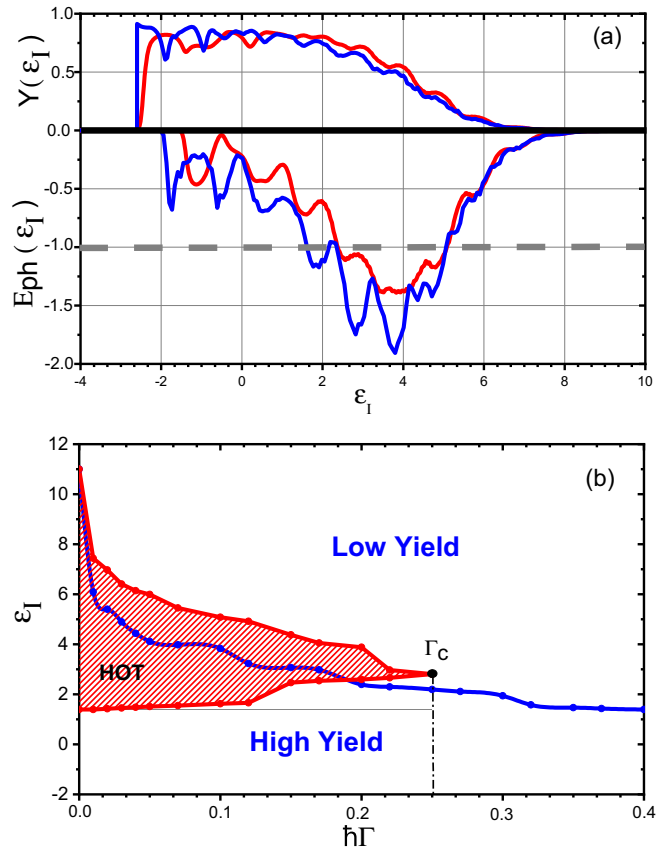

FIG. 4. Panel (a) shows the quantum yield $Y(\varepsilon_I)$ and the average energy $E_{ph}(\varepsilon_I)$ lost on the CTS, with recombination $\hbar\Gamma = 0.1$ and for $V = 0$ (red) and $V = 1.5$ (blue). The horizontal dashed gray line indicates the limit of vibrationally cold and hot CTS regimes. Panel (b) is a phase diagram as a function of the incident energy ε_I and of the recombination rate Γ for $V = 1.5$. It shows the zones of high yield ($Y > 0.5$) or low yield ($Y < 0.5$) and the zones of vibrationally hot CTS (red) or cold CTS (white).

values of $V = 0$ and $V = 1.5$. When $\varepsilon_I \leqslant 2$ the recombination effect is moderate and the CTS is vibrationally cold. This regime is rather similar to the vibrationally cold state regime of Fig. 3 without recombination. When $\varepsilon_I \geqslant 2$ the quantum yield decreases with a vibrationally hot CTS regime. For even higher values of ε_I the average energy E_{TS} decreases meaning again a vibrationally cold CTS regime with a small quantum yield $Y < 0.5$. This results from a regime of tunneling. Indeed, the condition of energy conservation implies that the electron can enter the acceptor channels only after having excited several phonons. A simple physical image is that the excitation of several phonons, which is performed in a tunneling regime, requires a time that increases with ε_I. During this time there is a transfer in the recombination channels with small n at a constant rate Γ which leads to a smaller yield and smaller number of phonons emitted. We note that if there were additional electronic bands at higher energies in the acceptor the electron could be injected into these bands without exciting phonons. This could lead to an efficient injection with a high quantum yield for high injection energy. For example, the experimental results in [23] show that the efficiency of the injection does not depend on the injection

energy. These results are not compatible with the conclusions of our model, which suggests that the injection can be done in several electronic bands in the acceptor material for these systems.

In panel (b) of Fig. 4 the results for $V = 1.5$ are summarized in a phase diagram with the two variables ε_I and Γ. The red zone represents the vibrationally hot CTS cases with more than one phonon emitted and the white zone represents the vibrationally cold CTS regime. One sees that for sufficiently strong recombination $\Gamma > \Gamma_C$ there are no more values of ε_I leading to a vibrationally hot CTS. Note that for energies between -2 and $E_{\mathrm{Min}} \simeq -2.4$ (not shown here) the yield will decrease again and becomes zero if $\varepsilon_I < E_{\mathrm{Min}}$.

Several additional comments are useful. In the presence of electron-hole interaction localized states are created for which the electron is spatially close to the CTS. Despite these localized states it is possible to inject electrons at higher energies with a high yield. Indeed for a particle that is initially in a state (the LUMO orbital of the donor side) coupled to a continuum, this corresponds to a resonant injection into a continuum [45]. Note that if the hopping integral m had a finite value the localized states of the donor+acceptor system would have a finite component on the LUMO orbital by a hybridization effect. This has been discussed in [59]. In that case, the yield would be smaller than one even within the limit of vanishing recombination. Indeed the component of the initial state that is on the localized states cannot leave the interface. Therefore a too high value of the hopping integral m can be deleterious to the quantum yield due to the hybridization with the localized states. This may suggest a way to improve the quantum yield.

To conclude the present model shows that in a large range of incident energies ε_I, of the order of the pure electronic bandwidth $4J$, there can be a high quantum yield of injection and a vibrationally cold CTS despite the electron-vibration coupling. This is consistent with many experiments [19]. Therefore a vibrationally cold transfer state with a high yield is compatible with a strong electron vibration coupling which creates pseudogaps and polaronic states on the acceptor side. In addition, the model shows that the recombination process plays an essential role in the occurrence of vibrationally hot or cold charge transfer states. For large values of ε_I we show that the energy conservation imposes the injection to occur after several phonon excitations, which is a tunneling process. In this regime, the detailed characteristics of the recombination process have a strong influence on the quantum yield of the electron transfer. We emphasize that the present approach could be used to treat models with other characteristics, such as multiple vibration mode frequencies, multiple excitonic states, or complex bands in the acceptor. It should also be useful for transfer processes at interfaces in other photovoltaic systems or even in photosynthetic systems [60–62].

We would like to thank Xavier Blase, Guy Trambly de Laissardière, and Sonia Haddad for stimulating discussions. The numerical calculations have been performed at Institut Néel, Grenoble. We thank Patrick Belmain, computing center engineer, for computing assistance. A.P. thanks France 2030 QuantForm-UGA for support through a Ph.D. grant.

[1] J. Xue and J. Bao, Interfacial charge transfer of heterojunction photocatalysts: Characterization and calculation, Surf. Interfaces **25**, 101265 (2021).

[2] A. Yan, X. Shi, F. Huang, M. Fujitsuka, and T. Majima, Efficient photocatalytic H_2 evolution using $NiS/ZnIn_2S_4$ heterostructures with enhanced charge separation and interfacial charge transfer, Appl. Catal. B **250**, 163 (2019).

[3] C. Wang, X. Zhang, S. Liu, H. Zhang, Q. Wang, C. Zhang, J. Gao, L. Liang, and H. Cao, Interfacial charge transfer and zinc ion intercalation and deintercalation dynamics in flexible multicolor electrochromic energy storage devices, ACS Appl. Energy Mater. **5**, 88 (2022).

[4] J. Fujisawa, Interfacial charge-transfer transitions for direct charge-separation photovoltaics, Energies **13**, 2521 (2020).

[5] A. Uddin, Organic solar cells, in *Comprehensive Guide on Organic and Inorganic Solar Cells* (Elsevier, 2022), pp. 25–55.

[6] P. K. Nayak, S. Mahesh, H. J. Snaith, and D. Cahen, Photovoltaic solar cell technologies: Analysing the state of the art, Nat. Rev. Mater. **4**, 269 (2019).

[7] J. Zhang, X. Zhu, M. Wang, and B. Hu, Establishing charge-transfer excitons in 2D perovskite heterostructures, Nat. Commun. **11**, 2618 (2020).

[8] F. Gao and O. Inganäs, Charge generation in polymer-fullerene bulk-heterojunction solar cells, Phys. Chem. Chem. Phys. **16**, 20291 (2014).

[9] I. Etxebarria, J. Ajuria, and R. Pacios, Polymer:fullerene solar cells: Materials, processing issues, and cell layouts to reach power conversion efficiency over 10%, a review, J. Photonics Energy **5**, 057214 (2015).

[10] A. Karki, A. J. Gillett, R. H. Friend, and T. Q. Nguyen, The path to 20% power conversion efficiencies in nonfullerene acceptor organic solar cells, Adv. Energy Mater. **11**, 2003441 (2021).

[11] C. Deibel and V. Dyakonov, Polymer-fullerene bulk heterojunction solar cells, Rep. Prog. Phys. **73**, 096401 (2010).

[12] S. Ono and K. Ohno, Origin of charge transfer exciton dissociation in organic solar cells, in *Excitons*, edited by S. L. Pyshkin (IntechOpen, 2018).

[13] R. A. Street, M. Schoendorf, A. Roy, and J. H. Lee, Interface state recombination in organic solar cells, Phys. Rev. B **81**, 205307 (2010).

[14] C. Göhler, A. Wagenpfahl, and C. Deibel, Nongeminate recombination in organic solar cells, Adv. Electron. Mater. **4**, 1700505 (2018).

[15] X.Y. Zhu, Q. Yang, and M. Muntwiler, Charge-transfer excitons at organic semiconductor surfaces and interfaces, Acc. Chem. Res. **42**, 1779 (2009).

[16] T. M. Clarke and J. R. Durrant, Charge photogeneration in organic solar cells, Chem. Rev. **110**, 6736 (2010).

[17] S. D. Baranovskii, M. Wiemer, A. V. Nenashev, F. Jansson, and F. Gebhard, Calculating the efficiency of exciton dissociation at the interface between a conjugated polymer and an electron acceptor, J. Phys. Chem. Lett. **3**, 1214 (2012).

[18] P. K. Nayak, K. L. Narasimhan, and D. Cahen, Separating charges at organic interfaces: Effects of disorder, hot states, and electric field, J. Phys. Chem. Lett. **4**, 1707 (2013).

[19] H. Bässler and A. Köhler, "Hot or cold": How do charge transfer states at the donor-acceptor interface of an organic solar cell dissociate? Phys. Chem. Chem. Phys. **17**, 28451 (2015).

[20] S. Few, J. M. Frost, and J. Nelson, Models of charge pair generation in organic solar cells, Phys. Chem. Chem. Phys. **17**, 2311 (2015).

[21] G. D'Avino, Y. Olivier, L. Muccioli, and D. Beljonne, Do charges delocalize over multiple molecules in fullerene derivatives? J. Mater. Chem. C **4**, 3747 (2016).

[22] D. Brey, W. Popp, P. Budakoti, G. D'Avino, and I. Burghardt, Quantum dynamics of electron-hole separation in stacked perylene diimide-based self-assembled nanostructures, J. Phys. Chem. C **125**, 25030 (2021).

[23] B. R. Gautam, R. Younts, W. Li, L. Yan, E. Danilov, E. Klump, I. Constantinou, F. So, W. You, H. Ade *et al.*, Charge photogeneration in organic photovoltaics: Role of hot versus cold charge-transfer excitons, Adv. Energy Mater. **6**, 1301032 (2016).

[24] D. Lee, J. Lee, D. H. Sin, S. G. Han, H. Lee, W. Choi, H. Kim, J. Noh, J. Mun, W. Sung, *et al.*, Intrachain delocalization effect of charge carriers on the charge-transfer state dynamics in organic solar cells, J. Phys. Chem. C **126**, 3171 (2022).

[25] G. Grancini, M. Maiuri, D. Fazzi, A. Petrozza, H. J. Egelhaaf, D. Brida, G. Cerullo, and G. Lanzani, Hot exciton dissociation in polymer solar cells, Nat. Mater. **12**, 29 (2013).

[26] Z. Zheng, N. R. Tummala, Y. T. Fu, V. Coropceanu, and J. L. Brédas, Charge-transfer states in organic solar cells: Understanding the impact of polarization, delocalization, and disorder, ACS Appl. Mater. Interfaces **9**, 18095 (2017).

[27] V. P. Antropov, O. Gunnarsson, and A. I. Liechtenstein, Phonons, electron-phonon, and electron-plasmon coupling in C_{60} compounds, Phys. Rev. B **48**, 7651 (1993).

[28] F. Castet, G. D'Avino, L. Muccioli, J. Cornil, and D. Beljonne, Charge separation energetics at organic heterojunctions: On the role of structural and electrostatic disorder, Phys. Chem. Chem. Phys. **16**, 20279 (2014).

[29] G. D'Avino, L. Muccioli, F. Castet, C. Poelking, D. Andrienko, Z. G. Soos, J. Cornil, and D. Beljonne, Electrostatic phenomena in organic semiconductors: Fundamentals and implications for photovoltaics, J. Phys.: Condens. Matter **28**, 433002 (2016).

[30] S. Bera, N. Gheeraert, S. Fratini, S. Ciuchi, and S. Florens, Impact of quantized vibrations on the efficiency of interfacial charge separation in photovoltaic devices, Phys. Rev. B **91**, 041107(R) (2015).

[31] L. Onsager, Deviations from Ohm's law in weak electrolytes, J. Chem. Phys. **2**, 599 (1934).

[32] L. Onsager, Initial recombination of ions, Phys. Rev. **54**, 554 (1938).

[33] R. A. Marcus, On the theory of oxidation-reduction reactions involving electron transfer. I, J. Chem. Phys. **24**, 966 (1956).

[34] D. Fazzi, M. Barbatti, and W. Thiel, Hot and cold charge-transfer mechanisms in organic photovoltaics: Insights into the excited states of donor/acceptor interfaces, J. Phys. Chem. Lett. **8**, 4727 (2017).

[35] X. K. Chen, V. Coropceanu, and J. Brédas, Assessing the nature of the charge-transfer electronic states in organic solar cells, Nat. Commun. **9**, 5295 (2018).

[36] S. Tscheuschner, H. Bässler, K. Huber, and A. Köhler, A combined theoretical and experimental study of dissociation of charge transfer states at the donor-acceptor interface of organic solar cells, J. Phys. Chem. B **119**, 10359 (2015).

[37] S. Athanasopoulos, S. Tscheuschner, H. Bässler, and A. Köhler, Efficient charge separation of cold charge-transfer states in organic solar cells through incoherent hopping, J. Phys. Chem. Lett. **8**, 2093 (2017).

[38] T. Fujita, M. K. Alam, and T. Hoshi, Thousand-atom ab initio calculations of excited states at organic/organic interfaces: Toward first-principles investigations of charge photogeneration, Phys. Chem. Chem. Phys. **20**, 26443 (2018).

[39] G. Wellein and H. Fehske, Polaron band formation in the Holstein model, Phys. Rev. B **56**, 4513 (1997).

[40] J. Ku, Y. Lansac, and Y. H. Jang, Time-dependent density functional theory study on benzothiadiazole-based low-band-gap fused-ring copolymers for organic solar cell applications, J. Phys. Chem. C **115**, 21508 (2011).

[41] C. Andrea Rozzi, S. Maria Falke, N. Spallanzani, A. Rubio, E. Molinari, D. Brida, M. Maiuri, G. Cerullo, H. Schramm, J. Christoffers, *et al.*, Quantum coherence controls the charge separation in a prototypical artificial light-harvesting system, Nat. Commun. **4**, 1602 (2013).

[42] M. Polkehn, P. Eisenbrandt, H. Tamura, and I. Burghardt, Quantum dynamical studies of ultrafast charge separation in nanostructured organic polymer materials: Effects of vibronic interactions and molecular packing, Int. J. Quantum Chem. **118**, e25502 (2018).

[43] D. E. Wilcox, M. H. Lee, M. E. Sykes, A. Niedringhaus, E. Geva, B. D. Dunietz, M. Shtein, and J. P. Ogilvie, Ultrafast charge-transfer dynamics at the boron subphthalocyanine chloride/C_{60} heterojunction: Comparison between experiment and theory, J. Phys. Chem. Lett. **6**, 569 (2015).

[44] Y. Zhao and W. Liang, Charge transfer in organic molecules for solar cells: Theoretical perspective, Chem. Soc. Rev. **41**, 1075 (2012).

[45] H. Vázquez and A. Troisi, Calculation of rates of exciton dissociation into hot charge-transfer states in model organic photovoltaic interfaces, Phys. Rev. B **88**, 205304 (2013).

[46] C. Faber, J. L. Janssen, M. Côté, E. Runge, and X. Blase, Electron-phonon coupling in the C_{60} fullerene within the many-body *GW* approach, Phys. Rev. B **84**, 155104 (2011).

[47] R. Haydock, The recursive solution of the Schrödinger equation, in *Solid State Phys.*, Vol. 35 (Elsevier, 1980), pp. 215–294.

[48] S. Katsura and M. Takizawa, Bethe lattice and the Bethe approximation, Prog. Theor. Phys. **51**, 82 (1974).

[49] See Supplemental Material at http://link.aps.org/supplemental/10.1103/PhysRevB.106.195420 for technical details and additional results.

[50] T. Holstein, Studies of polaron motion: Part I. The molecular-crystal model, Ann. Phys. **8**, 325 (1959).

[51] T. Holstein, Studies of polaron motion: Part II. The "small" polaron, Ann. Phys. **8**, 343 (1959).

[52] T. Nemati Aram, P. Anghel-Vasilescu, A. Asgari, M. Ernzerhof, and D. Mayou, Modeling of molecular photocells: Application to two-level photovoltaic system with electron-hole interaction, J. Chem. Phys. **145**, 124116 (2016).

[53] G. Wellein and H. Fehske, Self-trapping problem of electrons or excitons in one dimension, Phys. Rev. B **58**, 6208 (1998).

[54] S. Ciuchi, F. de Pasquale, S. Fratini, and D. Feinberg, Dynamical mean-field theory of the small polaron, Phys. Rev. B **56**, 4494 (1997).

[55] E. V. L. de Mello and J. Ranninger, Dynamical properties of small polarons, Phys. Rev. B **55**, 14872 (1997).

[56] K. D. Richler, S. Fratini, S. Ciuchi, and D. Mayou, Inhomogeneous dynamical mean-field theory of the small polaron problem, J. Phys.: Condens. Matter **30**, 465902 (2018).

[57] L. Zhang, Y. Hao, and K. Gao, Efficient quantum theory for studying cold charge-transfer state dissociations in donor-acceptor heterojunction organic solar cells, Appl. Phys. Lett. **117**, 123301 (2020).

[58] K. Chika, A. Perrin, J. Jemaa Khabthani, J. P. Julien, S. Charfi Kaddour, and D. Mayou, The embedded charge transfer state model (unpublished).

[59] G. Jemaï, K. Chika, J. J. Khabthani, and D. Mayou, Influence of the electron-vibration coupling on the interfacial charge transfer in organic solar cells: A simple quantum model, J. Phys.: Condens. Matter **34**, 425001 (2022).

[60] Y. Song, R. Sechrist, H. H. Nguyen, W. Johnson, D. Abramavicius, K. E. Redding, and J. P. Ogilvie, Excitonic structure and charge separation in the heliobacterial reaction center probed by multispectral multidimensional spectroscopy, Nat. Commun. **12**, 2801 (2021).

[61] C. Schwarz, S. Tscheuschner, J. Frisch, S. Winkler, N. Koch, H. Bässler, and A. Köhler, Role of the effective mass and interfacial dipoles on exciton dissociation in organic donor-acceptor solar cells, Phys. Rev. B **87**, 155205 (2013).

[62] S. N. Hood and I. Kassal, Entropy and disorder enable charge separation in organic solar cells, J. Phys. Chem. Lett. **7**, 4495 (2016).